J. Min. Metall. Sect. B-Metall. 59 (2) (2023) 217 - 229

Journal of Mining and Metallurgy, Section B: Metallurgy

INFLUENCE OF THERMAL AGEING ON TENSILE-PLASTIC FLOW AND WORK HARDENING PARAMETERS OF INDIAN REDUCED ACTIVATED FERRITIC MARTENSITIC STEEL

K.C. Sahoo [a, b, *], K. Laha [b]

[a] Indira Gandhi Institute of Technology, Sarang, India
[b] Metallurgy and Materials Group, Indira Gandhi Centre for Atomic Research, Kalpakkam, India

(Received 14 November 2022; Accepted 25 July 2023)

Abstract

The present study investigates the influence of thermal ageing (873K/5000h) on the microstructure, tensile-plastic flow behavior, and work hardening parameters of normalized and tempered (N&T) 1.4W-0.06Ta Indian Reduced Activated Ferritic Martensitic (INRAFM) steel. To comprehensively understand the tensile-plastic flow response of the INRAFM steel across a broad temperature spectrum of 300-873 K, the Hollomon, Ludwigson and Voce equations were employed. The results reveal an augmentation in the strain hardening exponent following the ageing process, attributed to the heightened work hardening capability of the aged steel, while the strain hardening coefficient exhibited a decline post ageing. To elucidate the dislocation debris structure's formation and movement within both the N&T and thermally aged specimens, transmission electron microscopy (TEM) specimens were procured in close proximity to the tensile tested specimens at varying temperatures of 300, 573 and 873 K. The tensile plastic flow behavior at diverse temperatures was aptly described by Hollomon, Ludwigson, and Voce equations. The fitting accuracy of these equations was determined using the goodness of fit, as indicated by the lowest χ^2 values. The constitutive Voce equation successfully captured the yield strength (YS) and ultimate tensile strength (UTS) with the initial stress and saturation stress acting as fitting parameters. Distinct patterns of initial stress and saturation stress variations were observed concerning both N&T and aged steel in relation to temperature. Furthermore, absolute value of the Voce strain component (n_v) demonstrated a reduction consequent to ageing, manifesting a two-stage behavior corresponding to temperature elevation. Notably, the deceleration of the recovery process during high temperature conditions was more pronounced in the thermally aged steel when contrasted with the N&T steel. Conclusively, the Voce relation proved efficacious in predicting the yield stress (YS) and ultimate tensile strength (UTS) of both the thermally aged and N&T INRAFM steel at varying temperatures.

Keywords: *Indian reduced activated ferritic martensitic steel; Thermal ageing; Electron microscopy studies; Tensile-plastic flow behavior; Ludwigson and Voce relation*

1. Introduction

Fusion energy is one of the long term, abundant and sustainable new clean energy sources that can solve the energy crisis of the whole world. India is one of the countries involved not only in the manufacturing and development but also in the testing of the Test Blanket Module (TBM) International Thermonuclear Experimental Reactor (ITER) [1]. The D-T fueled tokamak [2] is considered the most important candidate for fusion power generation. However, the problem of high energy neutron irradiation causes significant damage to the structural materials employed in the blanket module. Although conventional austenitic stainless steel has high temperature resistance and does not exhibit a sharp transition temperature from ductile to brittle, the problem of helium embrittlement and void swelling play a major drawback its use in fusion reactors [3]. Furthermore, the Cr-Mo steels are not suitable for use in fusion reactors due to the high energy neutron flux environment which produces radioactive nuclei such as Tc and Co^{60} in the long term due to the breeding effect of radioactive constituent such as Mo and Nb, respectively [4]. Therefore, a new variety of steel named low activation steel was developed by carefully selecting alloying elements with low activation potential, such as Fe, Cr, V, Ti, W, Si, C and keeping a strict control of elements that promote embrittlement, such as S, P,As, Sb, Sn, Zr and O [5-7]. 9Cr-RAFM steels are a modified version of ferritic Fe-(8-12)Cr-(1-2) Mo steels by interchanging Mo and Nb with W and Ta and other radioactive elements were reduced to a minimun to make the material as

Corresponding author: kanhu2011.sahoo@gmail.com

https://doi.org/10.2298/JMMB221114019S

low in activation as possible and to provide the same mechanical and thermal strength. Ferritic-martensitic reduced activation steel (RAFM) (9-12Cr-W-Ta-V), having tempered martensite microstructure is one of the possible structural material for the blanket module of fusion reactor. Several variety of RAFM steels were developed by different countries such as ORNL9Cr-2WVTa [8], F82H [9], EUROFER-97 [10] by the USA, Japan and European countries, respectively. In all the above mentioned steels, both YS and UTS were found to decrease due to ageing and the decrease was more dependent on temperature rather than time duration.

For the study of mechanical properties of structural material in high temperature applications, it is crucial to investigate the tensile, creep and fatigue properties at elevated temperatures. However, the present study involves the investigation of the work-hardening behavior of the material by analyzing the true plastic stress with true plastic strain for both N&T and thermally aged steel at different temperatures. It is also necessary to review the tensile strength and work hardening behavior of other ferritic steel grades at different temperatures. The work hardening behaviour of 9Cr-1Mo ferritic steel shows a gradual decrease in values from room temperature to 473 K followed by a plateau at intermediate temperatures and a rapid decrease at high temperatures.

The occurrence of a plateau at the intermediate temperature is due to the dominance of dynamic strain ageing (DSA) at the intermediate temperatures [11]. Ferritic/martensitic Fe-9Cr-2W-based steels also exhibited DSA effect at different strain rates (from 10^{-2} -$10^{-4}s^{-1}$) in the temperature range of 573 to 773 K. The YS and UTS were also plateaued at the same intermediate temperatures and at a strain rate of $10^{-4}s^{-1}$, both YS and UTS were higher at 673 K than at 623 K but overall YS and UTS were found to decrease with the increase in temperature [12]. Similar observations were made for RAFM steel, where both the yield stress and ultimate tensile strength of the steel decreased with temperature with a relatively slower rate of decrease at the intermediate temperature range. The DSA effect at the intermediate temperature results a negative sensitivity to strain rate. In addition, with the increase in strain rate tensile strength of the steel was also found to increase [13].

The tensile flow curve of many metals in the region of homogeneous plastic deformation can be represented by a simple Hollomon power law relation:

$$\sigma = K_H \varepsilon^{n_H} \tag{1}$$

A log-log plot of this equation-1 will generate a straight line with slope 'n_H' known as the strain hardening exponent, and intercept 'K_H', known as the strength coefficient. This type of relation is also known as Hollomon power law relation [14].

However, most FCC metals and their alloys have low stacking fault so the Holloman relation alone cannot adequately describe the flow curve of this type of metals. For this reason, Ludwigson [15] introduced a positive stress shift expression from the Hollomon relation to satisfactorily describe the plastic flow behavior of the FCC metals and alloys. It can be conquered by a supplementary term as

$$\sigma = K_1 \varepsilon^{n_1} + \exp\left(K_2 + n_2 \varepsilon\right) \tag{2}$$

Where 'K_1' and '' are the same as 'K_H' and 'n_H' in the Hollomon relation (Eq. 1), respectively, and 'K_2' and 'n_2' are additional constants.

Voce [16] [17] proposed a flow relationship for the metals exhibiting saturation stress at high stress/strain levels as. It can be conquered by adding another supplementary expression as given below

$$\sigma = \sigma_s - \left(\sigma_s - \sigma_i\right) exp\left[-\left(\varepsilon - \varepsilon_i\right) \Big/ \varepsilon_c\right] \tag{3}$$

Where 'σ_s' is the saturation stress, 'σ_i' and 'ε_i' are true stress and true plastic strain at the onset of plastic deformation, respectively, and 'ε_c' is a constant. In literatures 'σ_i' has been reported as initial stress. For situation $\varepsilon_i = 0$ above equation converts to

$$\sigma = \sigma_s - \left(\sigma_s - \sigma_i\right) exp\left(n_v \cdot \varepsilon\right) \tag{4}$$

Here $n_v = \dfrac{-1}{\varepsilon_c}, n_v$ decides the rate with which the stress attains steady state value.

In general, the application of the above tensile flow relations depends on the choice of materials, temperature and strain rate, which alters the shape of the stress-strain curve. For 316LN stainless steel, it was observed that the Ludwigson equation best described the tensile plastic flow behavior at 300 K, whereas in the intermediate temperature range (i.e. 523–723 K), both the Ludwigson and Voce equations provided lowest χ^2 values [18]. In the temperature range of 823–1023 K, Voce described the flow behaviour most accurately, while at further higher temperatures (1073 and 1123 K) the Hollomon equation followed stress–strain data more closely than other equations. However, for 9Cr–1Mo steel, the Ludwigson equation most accurately described tensile flow behavior of the steel in the temperature range 300–793 K. At high temperatures (723–873 K), the Ludwigson equation reduces to the Hollomon relation [19].

For IN-RAFM steel, Vanaja et.al. used Voce's constitutive equation to describe the tensile flow behavior and predict the tensile properties of the RAFM steel at different strain rates [13]. IN-RAFM steel was developed in IGCAR, Kalpakkam, with the careful optimization of W and Ta for greater

conjunction of physical and mechanical properties. INRAFM has a complex microstructure which causes degradation in microstructural and mechanical properties during thermal exposure at high temperature. For this reason, a better study of tensile-plastic flow and work hardening behavior of metals at high temperatures is necessary to accurately control material fabrication and ensure shield conduction during service. In this work, the effect of thermal ageing (873K for 5000 hours) of IN-RAFM steel (1.4W-0.06Ta) on the plastic flow and work hardening behavior of the steel was examined from 300 K to 873 K. In addition, studies were conducted to tie in the microstructure with the plastic flow and work hardening behavior of N&T and aged steel.

2. Experimental

The IN-RAFM steel ingots with a composition of 1.4W-0.06Ta were produced by vacuum induction melting and vacuum arc refining with the raw material suitably collected and careful command of radioactive tramp elements (Mo, Nb, B, Cu, Ni, Al, Co and Ti) and embritlling elements such as S, P, As, Sb, Sn, Zr and O by limiting them to ppm levels. The RAFM steel in the form of plates was provided by M/s. Mishra Dhatu Nigam Limited (MIDHANI), Hyderabad, India. The ingot was produced by vacuum induction melting followed by vacuum arc refining processes. The ingot was hot-forged and subsequently rolled to a 12 mm thick plate. The steel plates were subjected to the final heat treatment consisting of normalization at 1250 K for 30 min followed by tempering at 1033 K for 90 min. Table-1 shows the chemical composition of the INRAFM steel in the as-received condition.

In the present study, the N&T steel was thermal aged at 873 K for 5000 hours in a muffle furnace. The gauge length of the specimen was parallel to the rolling direction of the plate. Here, miniaturized flat specimen was used to study tensile deformation (Fig. 1). Tensile tests were performed at a temperature 298-873 K and a nominal strain rate of 3×10^{-4} s^{-1} using Hung Ta 2402 screw driven system fitted with a three zone furnace with an accuracy of ±2K temperature controller and a digital data acquisition system. The true stress (s) and true plastic strain (ε) data were obtained using a computer program coded software (ORIGIN 2015) from the digitized load–elongation data up to the maximum load values and were used for fitting to the Hollomon, Ludwigson and Voce constitutive equation of tensile flow. Since no strain gauge was used, the cross head displacement was taken as the specimen extension.

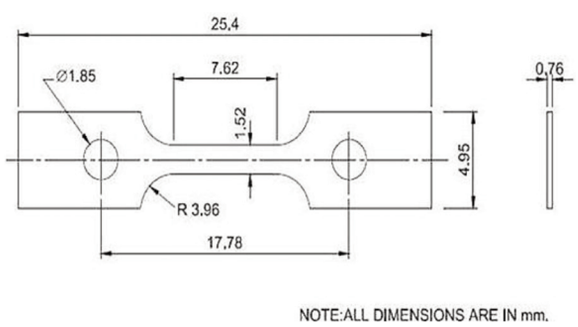

Figure 1. *Simplified diagram of miniaturized specimen used for tensile study*

The validity at different temperatures was concluded by the low value of the chi square (χ^2) and by the smallest error band in the evaluation of the constants of the constitutive equation. Chi square (χ^2) value is the sum of the squares of the deviations of the calculated stress values from the experimental stress values. For transmission electron microscopy (TEM), thin foils of with a thickness of about 100 μm were prepared by mechanical thinning followed by jet thinning. For jet thinning, 90% ethanol and 10% perchloric acid were used as electrolytes. TEM characterization was used at an accelerate voltage of 200 kV to study the defect structure near the failure location of the tensile tested specimens using CM 200 TEM (M/s FEI, the Netherland) machine. Image-J software was used to calculate the percentage of defect areas in the TEM images of the specimens tested at different temperatures.

3. Results and Discussion

3.1. Microstructure of N&T and aged steel

[Fig. 2(a, b)] and [Fig. 2(c, d)] show the optical and SEM micrographs of INRAFM steel under N&T and thermally aged steel. The micrograph observations reported that the steel has a rather complex microstructure. Careful examination of the microstructure by optical and SEM micrographs shows that the material has a tempered martensitic structure with earlier austenite grain boundaries followed by blocks and packets inside it. Most $M_{23}C_6$ precipitates are nicely decorated at each boundary and fine particles are present intergranularly.

Further examination by TEM shows that the steel has lath boundaries with relatively coarser particles and

Table 1. *Chemical compositions (Wt %) of the 1.4W-0.06Ta RAFM steels*

Elements	Cr	C	Mn	V	W	Ta	N	O	P	S
wt. %	9.03	0.126	0.56	0.24	1.39	0.06	0.03	0.002	<0.002	<0.001
Elements	B	Ti	Nb	Ni	Cu	Al	Si	Co	As+Sn+Sb	
wt. %	<0.0005	0.005	0.001	0.005	0.002	0.0035	0.06	0.005	<0.004	

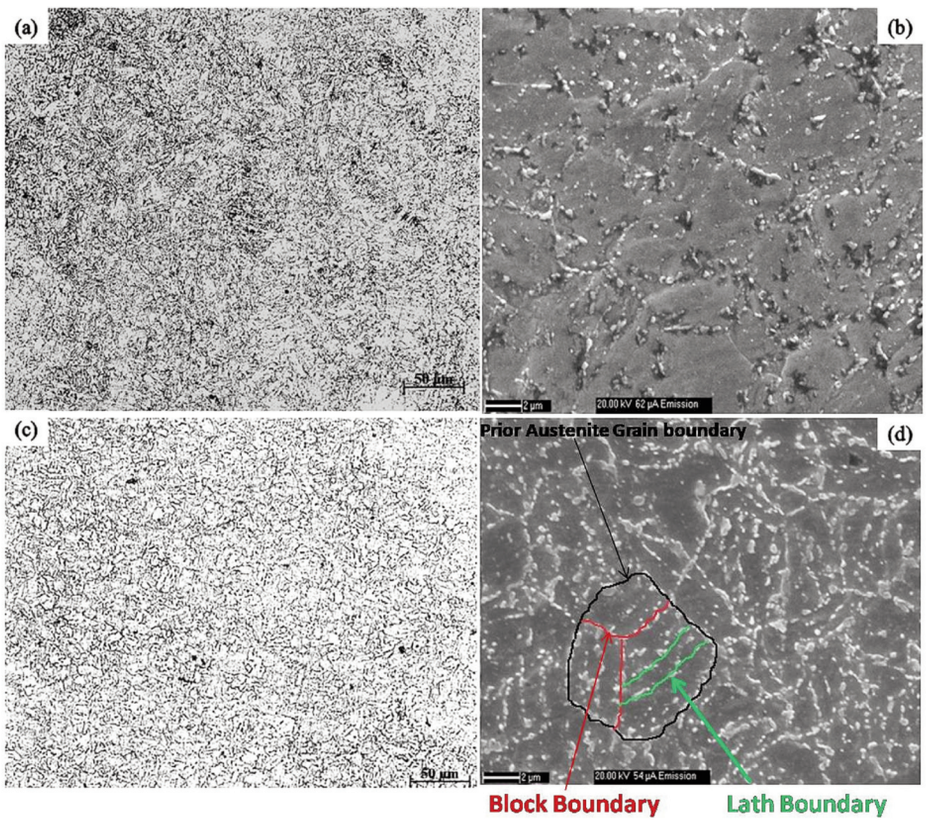

Figure 2. *(a) Optical and (b) SEM microstructure of N&T and (c) Optical and (d) SEM microstructure of thermal aged INRAFM steel*

fine particles inside the lath. It is well established in the literature that relatively coarser, elliptical particle with high aspect ratio at the sub-boundaries are chromium-rich $M_{23}C_6$ precipitate with tungsten and iron in solid solution [20]. The fine intragranular precipitates are vanadium and tantalum-rich carbides. It was observed that the average lath size was about 0.2 µm, and the precipitate size of $M_{23}C_6$ and MX was about 80 and 20 nm in N&T steel (Fig. 3(a)). After ageing for 5000h, the average lath size increased to about 0.35 µm. The MX nano-particles are enriched with Ta and V and were almost stable up to ~22 nm in comparison to N&T steel, while average size of $M_{23}C_6$ type precipitates (typically $Cr_{23}C_6$) was about 120 nm (Fig. 3(b)). The coarsening of the $Cr_{23}C_6$ precipitate is due to the depletion of chromium and carbon element from the surrounding matrix due to ageing and their coalescence with the existing $Cr_{23}C_6$ precipitate by Ostwald ripening mechanism, and by this process the concentration of tungsten increases in the matrix which is precipitated as Fe_2W. Fig. 3(c) shows EDS spectrum for the presence of $Cr_{23}C_6$ precipitate at the lath boundary. This phenomenon causes the favorable condition for the nucleation of Laves phase in the form of Fe_2W. In the previous paper it was observed that Laves phase with an average size of about 0.2 µm can also be observed during thermal ageing of INRAFM steel for 5000 h [20]. The reduction in dislocation density [Fig. 3(b)] is due to the acceleration of the recovery mechanism due to ageing. Fig. 3(c) shows generalized microstructure of INRAFM steel. From the SEM micrograph (Fig. 2(b, d)) it was observed that with ageing, prior austenite grain boundaries were not found to alter significantly.

3.2. True plastic stress-true plastic strain behavior

To study the response to work hardening at each test temperature, the true plastic stress and true plastic strain data were extracted from the yield strength data and the ultimate tensile strength from the true stress vs. true strain plot. In the previous studies, it was found that both yield strength and ultimate tensile strength decreased and ductility increased when aged for 5000h at 873 K [20]. It was reported that the decrease in tensile strength of the aged steel was due to the coarsening of $M_{23}C_6$ precipitates at the lath boundaries, the increase in cell size and the formation of the Laves phase. A similar observation was also reported by Falat et al. where an adverse effect on the tensile and fracture behavior of the martensitic (X10CrWMoVNb9-2)-bainitic (7CrMoVTiB10-10) steel pipe welds after isothermal ageing [21]. In addition, Dynamic Strain Ageing (DSA) was more pronounced in the case of aged steel at

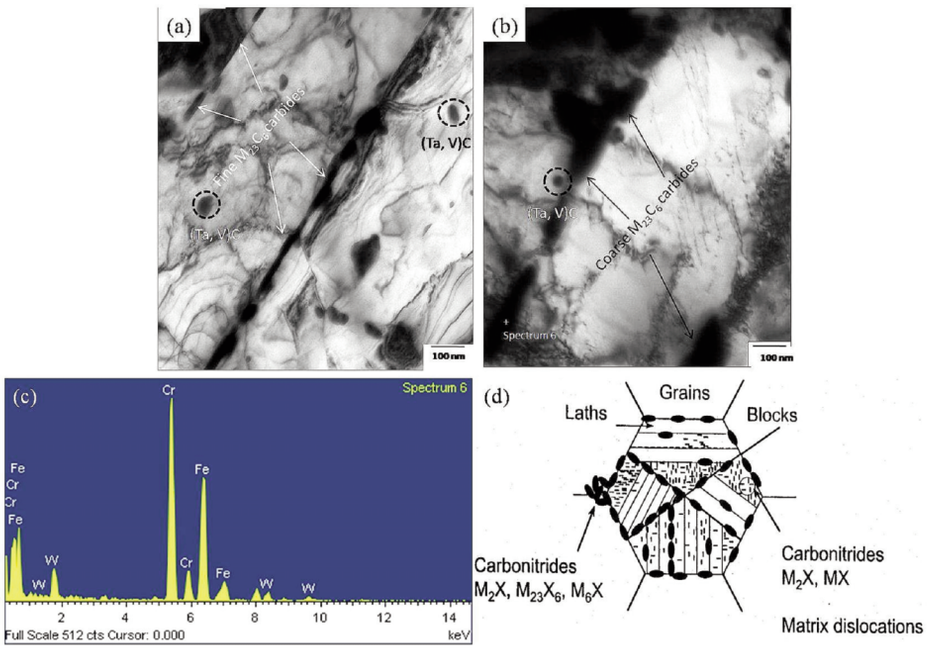

Figure 3. *TEM microstructure of (a) N&T and (b) thermal aged INRAFM steel and (c) EDS spectrum of $Cr_{23}C_6$ precipitate and (d) typical microstructure of INRAFM steel*

intermediate temperature (573 K) than N&T steel [20]. This is due to effective pinning of dislocation movement in aged steel than N&T steel, since thermal ageing causes annihilation of existing dislocations in ferritic-martensitic steel to some extent for which the remaining and new dislocations are able to move freely and can be effectively pinned by the formation of new and existing nano-precipitates. This leads to an increase in plastic flow behaviour at 573 K compared to 473 K. It will be interesting to see the variation in plastic flow behaviour of the material with temperature for N&T and aged steel and correlate the observations based on the microstructural aspect. It is also necessary to know the work hardening response of the thermally aged steel using different mathematical flow relationship at different service temperatures. Fig. 4(a) and 4(b) shows the variations of the experimental data for the true plastic stress with true plastic strain in log-log scale at a strain rate of $3\times10^{-4}s^{-1}$ for N&T and aged steel, respectively. From both the graphs, the variation of true plastic stress decreases with increasing temperature. However, in the moderate temperature range, a slight decrease in true plastic stress (due to DSA effect)was observed while in the high temperature regime (773-873K), a rapid decrease in flow stress value with increasing temperature was observed for both N&T and aged steel. Apart from the decrease in flow stress the range of true plastic strain also decreases with temperature. This is because of the decrease in work hardening region (i.e. the strain from YS to UTS) with increasing temperature. At elevated temperatures, thermally activated migration of atoms and vacancies, namely diffusion, occurs, which extensively increases the deformation rate compared to lower temperature, and makes the material start neck at

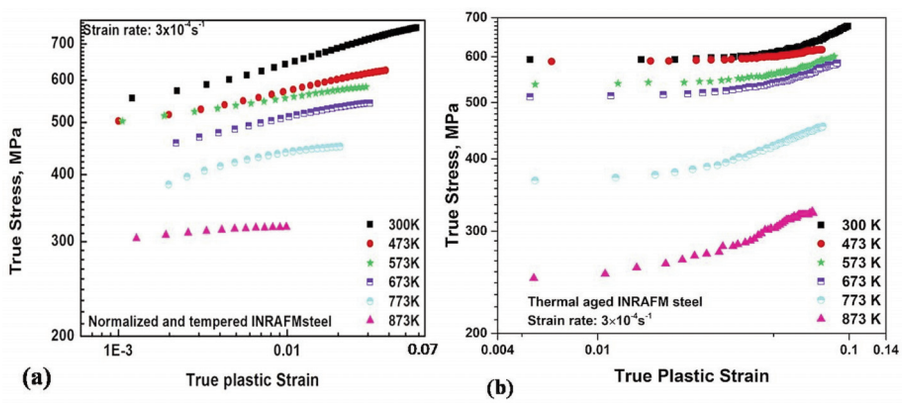

Figure 4. *Influence of temperature on true stress-true plastic strain at a strain rate of $3\times10^{-4}s^{-1}$ for (a) N&T steel (b) 5000h thermal aged steel*

low strains with lesser increase in stress.

At room and intermediate temperature, the log true stress-log true plastic strain data exhibits curvilinear behavior and approaches to linear behavior for higher temperature in both cases. Thermally aged steel shows a decrease in true stress and an increase in true plastic strain compared to N&T steel. The increase in plastic strain is due to the softening of the material and the increase in ductility due to the decrease in tensile strength after ageing.

TEM investigations were carried out near the tensile failure zone for both N&T and aged steel at room temperature, i.e., 300 K, 573 K, and 873 K to determine the nature of the dislocation movement. Different deformation behavior was observed for all specimens. At 300 K, both N&T and aged specimens shows restricted flow of deformation due to the absence of high temperature [Fig. 5(a, b)]. The restricted flow of deformation refers to the fact that the movement of the dislocations is obstructed by the presence of lath and packet boundaries due to the lack of thermal activation mechanisms in the matrix. At 300 K, the tested tensile aged steel showed a significant decrease in dislocation density which could be due to the thermal exposure (5000 hrs at 873 K) that generally results in a reduction in the dislocation density and precipitate coarsening compared to N&T steel [Fig. 5(b)].

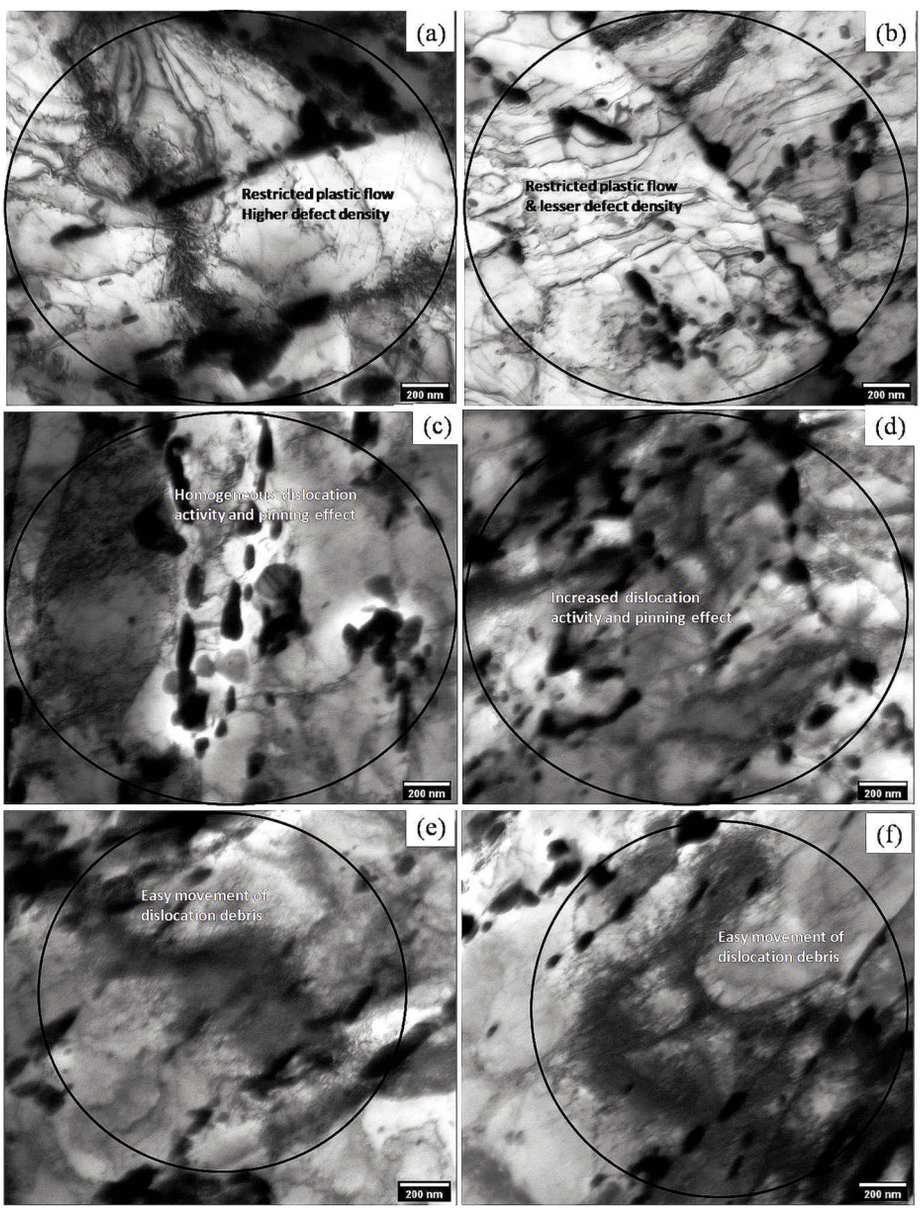

Figure 5. *TEM micrograph of tensile tested specimen: (a, c, e) represents TEM images for N&T steel at 300, 573 and 873 K respectively and (b, d, f) represents TEM images for aged steel at 300, 573 and 873 K respectively*

On the other hand, N&T steel at 573 K showed homogeneous distribution of dislocation activity region and pinning of dislocation movement by intragranular precipitates [Fig. 5(c)]. However, aged steel at 573 K showed both an increase in dislocation activity region and effective pinning of dislocation movement [Fig. 5(d)]. This could lead to a DSA effect in the thermally aged specimen at 573 K, and due to this, a slight increase in yield stress was observed in the aged steel compared to N&T steel [20]. At higher temperature (873 K), the N&T steel showed easy movement of dislocation debris without any effective obstacle [Fig. 5(e)]. A similar observation was also made for aged steel at 873 K; however, a lower dislocation density was observed compared to N&T steel [Fig. 5(f)]. This observation is plausible since the dislocation motion at higher temperatures is less likely to be pinned by the intragranular nanoprecipitates, resulting in an easy movement of the plastic flow.

The above observations were quantitatively measured by analyzing several TEM images under different tensile testing conditions using Image-J software. Fig. 6 shows the variation of defect area percentage at different temperatures for both N&T and thermally aged steel. The defect area percentage includes the sum of the area of free dislocations, dislocation cells, subgrain formation, and deformation bands relative to the total area of the matrix. During the analysis the area percentage of different precipitates was not included. It was observed that defect area percentage was significantly lower (about 15%) in the aged steel compared to N&T steel (about 27%) at 300 K tensile test temperature. However, at 573 K, the defect area percentage was slightly increased in the case of aged steel (about 44% for aged steel and 40% for N&T steel) which could be due to the DSA effect for the reasons mentioned above. The DSA effect in aged steel at 573 K was described in a previous paper [20]. With increasing temperature (at 673 K) the defect area percentage was about 38 % for N&T steel and 35% for aged steel. The dominance of dynamic recovery at high temperatures for N&T and aged steel could lead to a decrease in defect area percentage due to rapid decrease in the flow stress and work hardening parameters. Similarly, at 873 K, the defect area percentage was relatively higher for N&T steel (41%) than aged steel (about 31%). It is quite evident that an increase in temperature results in thermal activation of dislocations and that N&T steel generally has a higher percentage of dislocation density in as received conditions and the thermal aged specimen has a lower dislocation density because of annihilation of the dislocations due to thermal exposure.

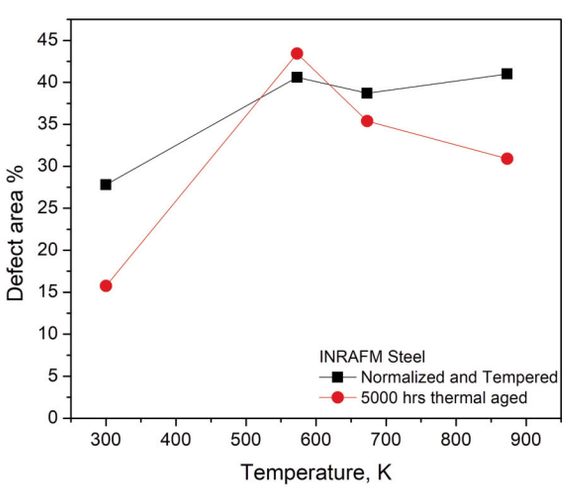

Figure 6. *Variation defect area percentage based on TEM with temperature of tensile tests of both N&T and thermal aged steels*

3.3. Applicability of different flow relationship by goodness of fit (χ^2)

The acceptability of different flow relationships viz. Hollomon, Ludwigson and Voce were evaluated based on the χ^2 values obtained at different temperatures for N&T and aged steel as shown in Table 2 and Table 3, respectively. The graphical variation of different flow relationships (Fig. 7(a, b, c, d)) shows that Hollomon equation shows highest χ^2 values at the room temperature and at 873K, it is comparable with Voce and Ludwigson relation in both N&T and aged conditions. Hollomon relation shows very high χ^2 values at room temperature for aged one than N&T steel (Fig. 7(b)).

Table 2. *Typical χ^2 values for different flow relationship at various temperatures for normalized and tempered steel at a strain rate 3×10^{-4} s^{-1}*

Temperature, K	χ^2 values		
Equations	Hollomon	Ludwigson	Voce
300	7.46	1.60	7.28
473	3.19	0.48	2.39
573	0.59	0.09	1.85
673	4.52	0.03	1.04
773	16.98	2.27	2.09
873	0.77	0.005	0.006

Table 3. *Typical χ^2 values for different flow relationship at various temperatures for thermal aged steel at a strain rate of 3×10^{-4} s^{-1}*

Temperature, K	χ^2 values		
Equations	Hollomon	Ludwigson	Voce
300	62.13	1.47	2.40
473	20.40	0.79	0.65
573	9.20	0.50	0.31
673	5.16	0.37	0.30
773	0.96	0.24	1.25

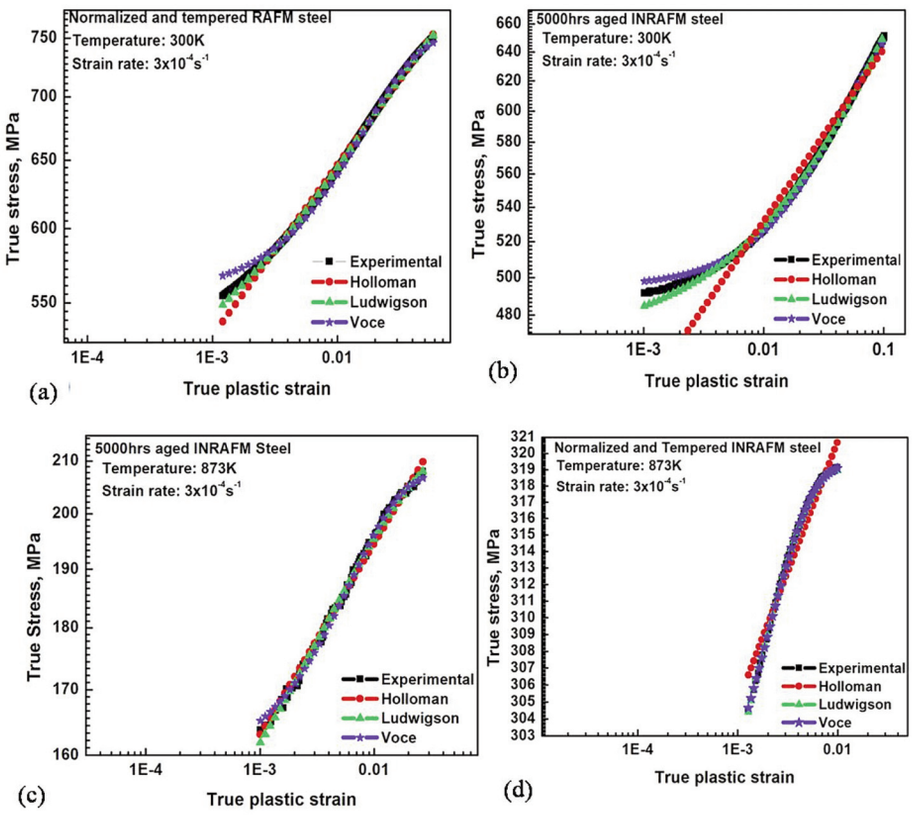

Figure 7. *True stress- true plastic strain for (a) N&T (b) 5000 hrs thermal aged steel at 300 K and (c) N&T (d) 5000 hrs thermal aged steel at 873 K at a strain rate of $3x10^{-4}$ s^{-1} for 1.4W-0.06Ta INRAFM steel*

Ludwigson relation provided the lowest χ^2 values at all temperatures for N&T steel and at low and high temperatures for aged steel. High χ^2 values at intermediate temperatures suggest the predominance of the DSA effect in aged steel at intermediate temperature in comparison to N&T steel. It was found that at highest temperature (873 K), the Voce relation showed a good correlation with the Ludwigson relation for both steels, while at intermediate temperatures the Voce relation provided lowest χ^2 values for the aged steel. This is due to the consideration of the initial stress in the Voce equation, which varies due to the DSA effect. All relationships show a large variation in χ^2 values between the N&T and aged steel corresponding to their temperature. For all the relationships, the N&T steel shows a good fit (Lowest χ^2 values) compared to the aged steel for the respective temperatures.

At the highest temperature, the Ludwigson relation reduces to the Hollomon relation following true stress–true plastic strain data more closely with low χ^2 values, as shown in Fig. 7(c, d). Hence, the combination of Hollomon and Ludwigson provides the most appropriate description of the true stress and true strain behavior. Although, the Voce equation provides higher χ^2 values than the combination of Hollomon and Ludwigson, it finds application for the following reasons: (a) single flow relation is able to adequately describe the true stress and true strain over a wide range of temperature, (b) prediction of tensile properties such as yield strength and ultimate tensile strength [22], (c) applicable to materials where saturation of stress is reached at relatively larger strains [23].

Different parameters are obtained from different power laws i.e. Hollomon, Ludwigson and Voce obtained on the bases of different temperature and ageing time. Since the Hollomon relation shows great variation in χ^2 values at room and intermediate temperature, it is not applicable to plastic flow behaviour.

3.4. Deviations of strain/work hardening parameters with temperature and ageing conditions

The dependence of the strain hardening exponent (n_1) and coefficient K_1 on temperature is shown in Fig. 8. Thermally aged steel displays an increasing trend of the value of 'n_1' with temperature compared to N&T steel (Fig. 8(a)). Ageing increases the work hardening capability of the steel, which is reflected in an increase in n_1 value. The dependence of n_1 on temperature revealed a continuous decrease from 300-

773K, followed by a rapid decrease at high temperature, i.e., at 873K for the N&T steel, while the thermally aged steel showed similar behavior as the N&T steel except at 573K (due to the DSA effect). Increase in value of n_1 for aged steel is due to the pinning of dislocation movement by the formation of new and existing precipitate. This causes restricted movement of the dislocation network structure and results in an increase in the work-hardening capability at intermediate temperatures [Fig. 5(d)].

Compared to 'n_1', a different trend was observed for 'K_1' with temperature. N&T steel showed a significant increase in the trend of K_1 with temperature compared to the aged condition (Fig. 8(b)). Ageing decreases the tensile strength of the steel, which causes a decrease in K_1 values. N&T steel exhibited a gradual decreasing trend from 300-573 K, followed by a plateau at 573-773 K and a rapid decrease at 873 K. A systematic decrease in K_1 was observed from 573-773 K, followed by a rapid decrease at the highest temperature in the case of aged steel.

Furthermore, a sharp increase in the absolute values of 'n_2' was observed with respect to their temperature due to thermal ageing (Fig. 8(c)). On the other hand, N&T steel exhibited a slight increase in the absolute values of 'n_2' when tested in the range of 300-573 K, followed by a rapid increase at 873 K, while thermally aged steel exhibited a slight increase in the absolute values of 'n_2' found in the range from 300-673 K, followed by a rapid increase from 673-873 K. The variation in 'n_2' indicated the extent of deviation from the Hollomon relation at low strains, and the high negative value of 'n_2' observed at high temperatures indicated the negligible second term of the Ludwigson relation at these temperatures. The increase in n_2 is due to the fact that the deformation becomes lighter with an increase in temperature due to the easy glide and cross-slip activity. It can be seen from fig. 8(d), that no change in K_2 values was observed with temperature due to ageing, except at 873 K, where a drastic reduction in K_2 values was observed due to ageing.

3.5. Variation of Voce constitutive parameter with temperature

Fig. 9(a), (b), (c) shows the variation of the Voce's constitutive equation parameters σ_i, σ_s and n_v with temperature for the N&T steel and with the aged condition, respectively. Both the initial stress (σ_i) and the saturation stress (σ_s) decrease continually with temperature for both steels (Fig. 9(a, b)). A slight increase in initial stress (σ_i) was observed at 573 K compared to 473 K due to DSA phenomenon(Fig. 9(a)) which is more pronounced in aged steel [24]. The decrease in σ_s with temperature suggests that stress saturation is reached at lower stresses, since

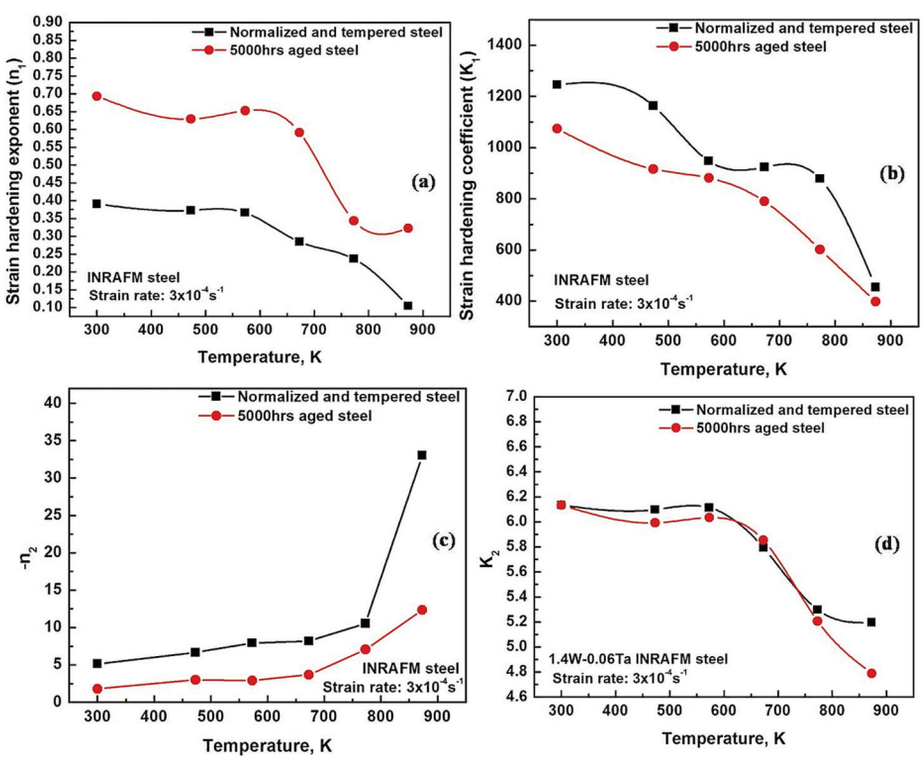

Figure 8. *The variation of (a) strain hardening exponent (n_1), (b) strain hardening coefficient (K_1), and (c) n_2 and (d) K_2 with temperature for N&T and thermal aged steel*

recovery is rapid with the rise in temperature (Fig. 9(b)). According to Kocks – Mecking [25] approach, during tensile deformation, the relative contention between generation and annihilation of dislocations is responsible for the saturation of the stress until instability or necking in the steel begins. According to Y. Estrin– Mecking [26] model, the interrelated primary deformation mechanisms developed from the steady state of dislocation substructure are responsible for the acquisition of both saturation stress obtained at constant strain rate during tensile test and the steady state strain rate achieved in the constant load creep test.

There was a slight decrease in both 'σ_i' and 'σ_s' with the effect of ageing. Due to ageing, the absolute variation of 'n_v' decreases compared to N&T steel (Fig. 9(c)). The absolute value of 'n_v' increases gradually with temperature from 300-673 K and then increases rapidly at higher temperature (673-873 K), indicating the acceleration of the recovery process controlled by dislocation climb and sub boundary migration. It was reported that the rate controlling deformation mechanism was invariably associated with 'n_v' [25, 26]. The dominance of cross slip leads to a low absolute value of n_v at low and medium temperatures, while the change in the controlling mechanism from cross slip to dislocation climb or formation and movement of dislocation debris and sub boundary migration (generated by dislocation loop formation) results in high absolute value of n_v at high temperatures [Fig. 5(e, f)].

Therefore, the dominance of formation and movement of dislocation debris along with dislocation climb at high temperature increases the absolute value of n_v in case of the N&T steel [Fig. 5(e)] compared to aged steel. In case of aged steel, because of the extensive precipitation on grain and grain boundary cross slip is difficult at intermediate temperature and climb is difficult at high temperature [Fig. 5(d)]. This could be the reason for the decrease in absolute values of n_v compared to N&T steel.

3.6 Relation between Voce's parameter and tensile strength

A good correlation between saturation stress (σ_s) and ultimate tensile strength (σ_u) was obtained using the Voce equation through equivalence relationship between 'σ_s' and the corresponding for both the N&T and aged steel at different temperatures (Fig.10(a)).

Mishra et al. [27] designed an expression to estimate 'σ_u' by invoking the Consideré criterion of instability at the onset of necking based on Voce's constitutive equation (3). By taking the differentiation of the Eq. (3) and replacing exp ($n_v\varepsilon$) with (σ-σ_s)/(σ_s-σ_i), we get;

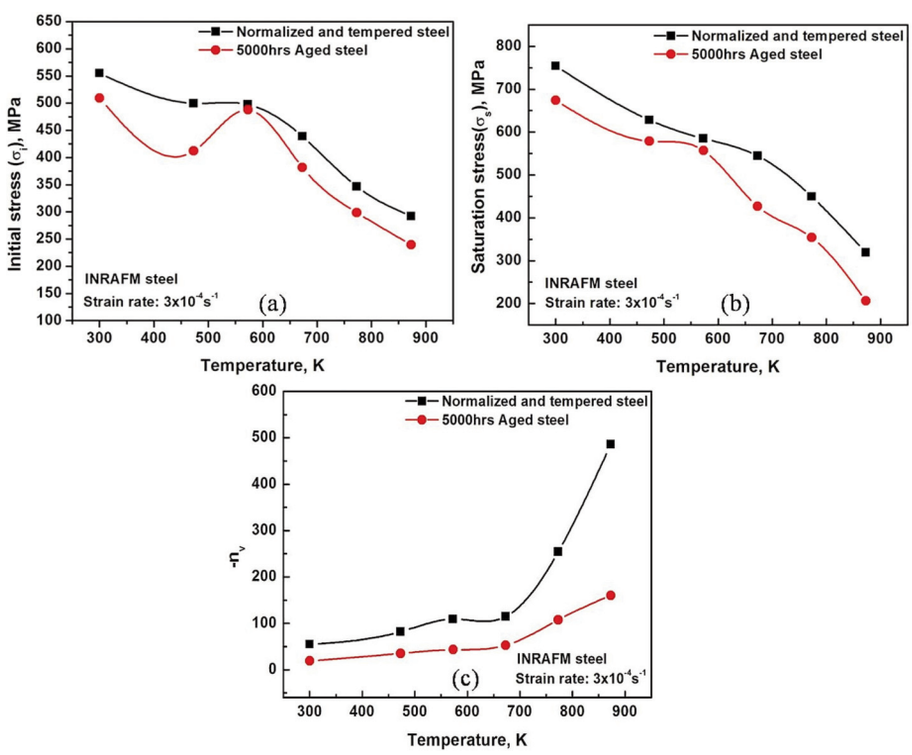

Figure 9. *The variation of Voce parameter (a) initial stress (σ_i), (b) saturation stress (σ_s) and (c) 'n_v' with temperature for N&T and thermal aged steel*

$$\Delta\sigma/\Delta\varepsilon = -n_v(\sigma_s - \sigma) \quad (5)$$

Again invoking Consideré criterion ($\Delta\sigma/\Delta\varepsilon$) by substituting with σ_{uv}, we get:

$$\sigma_{uv} = -n_v\sigma_s / (1 - n_v) \quad (6)$$

It was noticed that σ_u is linearly related to σ_{uv} for both N&T and aged steel by σ_u = 0.98486 σ_{uv} +10.02631 with correlation coefficient 0.995.

Like σ_u vs σ_{uv} the dependence of the Voce parameter (σ_i) on the true yield strength can be plotted because σ_i is the initial stress at the start of zero plastic strain. Fig. 10(b) compares the variation of σ_i with the true yield strength for both the N&T and aged steel. It was observed that the true yield strength is linearly related to σ_i for both N&T and aged steel by YS = 0.93923σ_i - 2.52683 with a correlation coefficient of 0.899. The obtained correlation coefficient suggests that the true yield stress is not so well correlated with the initial stress (σ_i). However, at lower and higher stresses, a good correlation is obtained for both steels, so that the prediction of the experimental yield stress is possible by knowing Voce's yield stress at lower and higher temperatures.

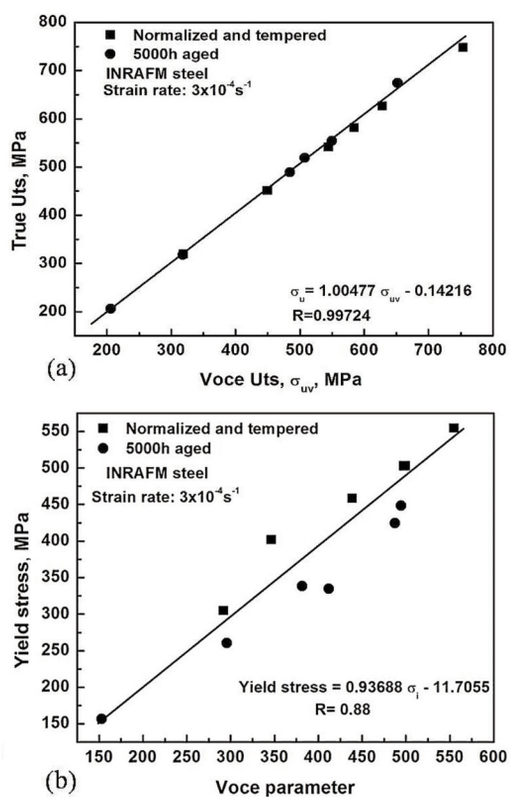

Figure 10. *Linear fit of the experimentally obtained (a) True UTS (σ_u) and Voce's UTS (σ_{uv}) and (b) True yield strength and Voce parameter (σ_i) for both N&T and thermal aged steels*

4. Conclusions

The important findings from the present investigations have been drawn as follows

Tensile flow behavior was adequately represented by both Ludwigson and Voce constitutive equation parameters. The Ludwigson relation provided the lowest χ^2 values at all temperatures for N&T steel and at low and high temperatures for thermally aged steel. At intermediate temperatures, the Voce relation provided the lowest χ^2 values for aged steel. At the highest temperature, the Ludwigson relation reduces to the Hollomon relation, which better follows true stress–true plastic strain data with low χ^2 values.

The variations of Ludwigson parameters (n_1, K_1, K_2) for both N&T and aged steel as a function of temperature exhibited a gradual decrease to plateaus at the intermediate temperature, followed by a rapid decrease at high temperatures (773-873 K). The presence of the DSA effect causes plateaus at intermediate temperature. The difference in the variation of n_1 between the N&T and aged steel at different temperatures was quite significant, while it was marginal for n_2 and no such difference was observed for K_2 except at 873 K. The variation of absolute values of n_2 showed a marginal increase in the temperature range from 300 to 573 K and a rapid increase at high temperatures (673-873 K). The increase in n_2 is due to ease of deformation due to easy glide and cross-slip activity with an increase in temperature.

The difference in tensile flow behavior of the material in both N&T and aged steel was correlated with the type of deformation induced dislocation substructure and the defect area percentage at different temperatures which showed a slight increase in the percentage of the defect area in aged steel at intermediate temperature (573 K).

The variation of Voce parameter σ_i and σ_s for both steels showed a gradual decrease for 300–473 K followed by plateaus, except for an increase in yield strength at 573 K for aged steel in the range 473–673 K and a sudden decrease at high temperatures. The occurrence of plateaus at intermediate temperatures is the presence of the DSA effect. The absolute value of 'n_v' increases gradually with temperature up to 673 K followed by a rapid increase at higher temperatures (673-873 K) indicating the decrease in cross slip, followed by an acceleration of the recovery process controlled by the dislocation climb and sub boundary migration. A good correlation was obtained for the true UTS (σ_u) with Voce UTS (σ_{uv}) and the initial stress (σ_i) with the true yield strength.

Acknowledgements

The authors acknowledge to department of

Metallurgy and Materials group of IGCAR, Kalpakkam for carrying out necessary experimental work and technical support during this investigation.

Data availability statement

The data cannot be made publicly available upon publication because they are not available in a format that is sufficiently accessible or reusable by other researchers. The data that support the findings of this study are available upon reasonable request from the authors.

Disclosure statement

No potential conflict of interest was reported by the authors.

References

[1] The ITER project. EFDA, European Fusion Development Agreement (2006).

[2] D. M. Meade, Tokamak fusion test reactor D-T results, Fusion Engineering Design, 30 (1995) 13-23. https://doi.org/10.1016/0920-3796(94)00398-Q

[3] P. Rodriguez, R. Krishnan, C.V. Sundaram, Radiation effects in nuclear reactor materials-correlation with structure, Bulletin Material Science, 6 (1984) 339–367. https://doi.org/10.1007/BF02743907

[4] B. Raj, T. Jayakumar, Development of reduced activation ferritic–martensitic steels and fabrication technologies for Indian test blanket module, Journal of Nuclear Material, 417 (2011) 72–76. https://doi.org/10.1016/j.jnucmat.2011.02.032

[5] R. L. Klueh, E.E. Bloom, The development of ferritic steels for fast induced-radioactivity decay for fusion reactor applications, Nuclear Engineering and Design, 2 (1985) 383–389. https://doi.org/10.1016/0167-899X(85)90026-6.

[6] R. Lindau R., M. Schirran, First results on the characterisation of the reduced-activation-ferritic-martensitic steel EUROFER, Fusion Engineering and Design, 58-59 (2001) 781–785. https://doi.org/10.1016/S0920-3796(01)00562-2

[7] A. Alamo, J. C. Brachet, A. Castaing, C. Lepoittevin, F. Barcelo, Physical metallurgy and mechanical behaviour of FeCrWTaV low activation martensitic steels: effects of chemical composition, Journal of Nuclear Material, 258–263 (1998) 1228–1235. https://doi.org/10.1016/S0022-3115(98)00190-1

[8] R. L. Klueh, M. A. Sokolov, Mechanical properties of irradiated 9Cr–2WVTa steel with and without nickel, Journal of Nuclear Material, 367 (2007) 102-106. https://doi.org/10.1016/j.jnucmat.2007.03.160.

[9] E. Wakai, M. Sato, T. Sawai, K. Shiba, S. Jitsukawa, Mechanical properties and microstructure of F82H steel doped with boron or boron and nitrogen as a function of heat treatment, Materials Transaction, 45 (2004) 407-410. https://doi.org/10.2320/matertrans.45.407

[10] K. Mergia, N. Boukos, Structural, thermal, electrical and magnetic properties of Eurofer 97 steel, Journal of Nuclear Material, 373 (2008) 1-8. https://doi.org/10.1016/j.jnucmat.2007.03.267

[11] J. Christophera, B.K. Choudharya, E.I. Samuela, V.S. Srinivasana, M.D. Mathew, Tensile flow and work hardening behaviour of 9Cr–1Mo ferritic steel in the frame work of Voce relationship, Materials Science and Engineering A, 528 (2011) 6589–6595. https://doi.org/10.1016/j.msea.2011.05.026

[12] K. He, Y. Wang, H. Wang, Influence of dynamic strain aging on ferritic/martensitic steel and stability analysis, Fusion Engineering and Design, 171 (2021) 112581. https://doi.org/10.1016/j.fusengdes.2021.112581

[13] J. Vanaja, K. Laha, S. Sam, M. Nandagopal, S.P. Selvi, M.D. Mathew, T. Jayakumar, E.R. Kumar, Influence of strain rate and temperature on tensile properties and flow behaviour of a reduced activation ferritic–martensitic steel, Journal of Nuclear Materials, 424 (2012) 116–122. https://doi.org/10.1016/j.jnucmat.2012.02.020.

[14] J. H. Hollomon, Tensile deformation, Transaction AIME, 162 (1945) 268-290.

[15] D. C. Ludwigson, Modified stress-strain relation for FCC metals and alloys, Metallurgical Transaction, 2(1971) 2825–2828. https://doi.org/10.1007/BF02813258

[16] E. Voce, The relationship between stress and strain for homogeneous deformation, Journal of Institute of Metal, 74 (1948) 537–562. https://cir.nii.ac.jp/crid/1573950400805224960

[17] E. Voce, A practical strain hardening function, Metallurgia, 51 (1955) 219–226. https://cir.nii.ac.jp/crid/1573668925830119040.

[18] B.K. Choudhary, E.I. Samuel, K.B. Rao, S.L. Mannan, Tensile stress–strain and work hardening behaviour of 316LN austenitic stainless steel, Material Science and Technology, 17 (2001) 223–231. https://doi.org/10.1179/026708301101509890

[19] D.P. Palaparti, B.K. Choudhary, E.I. Samuel, V.S. Srinivasan, M.D. Mathew, Influence of strain rate and temperature on tensile stress–strain and work hardening behaviour of 9Cr–1Mo ferritic steel, Materials Science and Engineering A, 538 (2012) 110–117. https://doi.org/10.1016/j.msea.2011.12.109

[20] K. C. Sahoo, J. Vanaja, P. Parameswaran, V. D. Vijayanand, K. Laha, Effect of thermal ageing on microstructure, tensile and impact properties of reduced activated ferritic-martensitic steel, Material Science & Engineering A, 686 (2017) 54–64. https://doi.org/10.1016/j.msea.2017.01.030

[21] L. Falat, L. Čiripová, V. Homolova, A. Kroupa, The influence of isothermal ageing and subsequent hydrogen charging at room temperature on local mechanical properties and fracture characteristics of martensitic-bainitic weldments for power engineering, Journal of Mining and Metallurgy, Section B: Metallurgy, 53 (2017) 373-382. https://doi.org/10.2298/JMMB170515033F

[22] A. Moitra, P. R. Sreenivasan, P. Parameswaran, S. L. Mannan, Dynamic deformation and fracture properties of simulated weld heat affected zone of 9Cr-1Mo steel from instrumented impact tests, Material Science and Technology, 18 (2002) 1195-1200. https://doi.org/10.1179/026708302225006106.

[23] A. Ghosh, A. Ray, D. Chakrabarti, C. L. Davis, Cleavage initiation in steel: Competition between large grains and large particles, Material Science &

Engineering A, 561 (2013) 126–135. https://doi.org/10.1016/j.msea.2012.11.019.

[24] R.W. Hayes, W.C. Hayes, A proposed model for the disappearance of serrated flow in two Fe alloys, Acta Metallurgica, 32 (1984) 259–267. https://doi.org/10.1016/0001-6160(84)90054-3.

[25] H. Mecking, U.F. Kocks, Kinetics of flow and strain-hardening, Acta Metallurgical and Materials, 29 (1981) 1865–1875. https://doi.org/10.1016/0001-6160(81)90112-7.

[26] Y. Estrin, H. Mecking, A unified phenomenological description of work hardening and creep based on one-parameter models, Acta Metallurgical and Materials, 32 (1984) 57–70. https://doi.org/10.1016/0001-6160(84)90202-5.

[27] N.S. Mishra, S. Mishra, V. Ramaswamy, Analysis of the temperature dependence of strain-hardening behavior in high-strength steel, Metallurgical Transaction A, 20 (1989) 2819–2829. https://doi.org/10.1007/BF02670174.

UTICAJ TERMIČKOG STARENJA NA PONAŠANJE PRI ZATEZNO-PLASTIČNOM TEČENJU I NA PARAMETRE OJAČAVANJA INDIJSKOG FERITNO-MARTENZITNOG ČELIKA NISKE AKTIVACIJE

K.C. Sahoo [a, b, *], K. Laha [b]

[a] Institut za tehnologiju Indire Gandi, Sarang, Indija

[b] Grupa za metalurgiju i materijale, Indira Gandi Centar za atomska istraživanja, Kalpakam, Indija

Apstrakt

Navedeno istraživanje proučava uticaj termičkog starenja na mikrostrukturu, ponašanje pri zatezno-plastičnom tečenju i parametre ojačavanja normalizovanog i temperovanog (N&T) 1.4W-0.06Ta indijskog feritno-martenzitnog čelika niske aktivacije (INRAFM), na temperaturi od 873 K tokom 5000 sati. Kako bi se sveobuhvatno razumeo odgovor čelika INRAFM na zatezno-plastično tečenje u širokom temperaturnom rasponu od 300-873 K, korišćene su Holomonove, Ludvigsonove i Voce jednačine. Rezultati pokazuju povećanje eksponenta ojačavanja usled procesa starenja, što se pripisuje povećanoj sposobnosti ojačavanja na starom čeliku. Suprotno tome, koeficijent ojačavanja usled procesa starenja pokazuje smanjenje. U cilju razjašnjenja formacije i pokreta strukture dislokacionog otpada kako kod N&T uzoraka tako i kod termalno starenih uzoraka, TEM uzorci su prikupljeni u neposrednoj blizini uzoraka testiranih na istezanje pri različitim temperaturama. Zatezno-plastično ponašanje pri različitim temperaturama adekvatno je opisano Holomonovim, Ludvigsonovim i Voce jednačinama. Tačnost prilagođavanja ovih jednačina određena je korišćenjem valjanosti podudaranja, kako je naznačeno najnižim vrednostima χ^2. Konstitutivna Voceova jednačina uspešno je prikazala granicu tečenja (YS) i zateznu čvrstoću pri istezanju (UTS), pri čemu su inicijalni napon i zasićeni napon delovali kao parametri prilagođavanja. Primećeni su jasni obrasci varijacija inicijalnog napona i zasićenog napona u vezi sa temperaturom kako kod N&T čelika, tako i kod starog čelika. Štaviše, apsolutna vrednost Voceovog komponentnog naprezanja (nv) pokazuje smanjenje usled starenja, ispoljavajući dvostepeno ponašanje u odnosu na povećanje temperature. Napomenuto je da je usporenje procesa oporavka pri visokim temperaturama bilo izraženije kod termički starenog čelika u poređenju sa N&T čelikom. Kao zaključak,Voce jednačina se pokazala uspešnom u prognoziranju granice tečenja (YS) i zatezne čvrstoće pri istezanju (UTS) kako kod termički starenog, tako i kod N&T INRAFM čelika pri različitim temperaturama.

Ključne reči: *Indijski feritno-martenzitni čelik niske aktivacije; Termičko starenje; Ispitivanja elektronskim mikroskopom; Ponašanje pri zatezno-plastičnom tečenju; Odnos Ludvigson i Voce jednačine*